PAPER

Check for updates

Three cobalt-based coordination polymers with tripodal carboxylate and imidazole-containing ligands: syntheses, structures, properties and DFT studies†

Long Tang, [ID] * Huan-Huan Wang, Yu-Hao Fu, Yi-Tong Wang, JiJiang Wang [ID] * and XiangYang Hou

Three cobalt-based coordination polymers [Co(Htatb)(1,3-bimyb)] (1), [Co(Htatb)(bimbp)]·DMF (2), and [Co(Htatb)(1,4-bimyb)]·H$_2$O (3) [H$_3$tatb = 4,4′,4″-s-triazine-2,4,6-tribenzoic acid, 1,3-bimyb = 1,3-bis(imidazole-1-ylmethyl)benzene, bimbp = 4,4′-bis(imidazolyl)biphenyl, 1,4-bimyb = 1,4-bis (imidazole-1-ylmethyl)benzene] were synthesized by hydrothermal reactions and characterized by single-crystal X-ray diffraction, thermogravimetric analyses, IR spectroscopy, UV-vis spectroscopy and elemental analysis. Compound **1** shows a double-strand chain structure, due to the intermolecular O−H···O hydrogen bonds and aromatic π−π stacking interactions, the adjacent chains are connected to produce a 3D supramolecular structure. Compound **2** shows a 2D structure with a 1D channel. Compound **3** displays a 2D layer structure, furthermore these layers are joined by O−H···O hydrogen bonding to generate a four-fold interpenetrating 3D architecture. The fluorescence properties of **1**–**3** and the magnetic behavior of **1** and **2** have also been investigated. Based on their crystal structures, compounds **1** and **2** were investigated using hybrid DFT methods at the B3LYP/6-31G (d) level. The DFT-BS approach was applied to study the magnetic coupling behavior. The results reveal that the calculated exchange coupling constants J were in good agreement with the experimental data.

1 Introduction

Metal–organic coordination polymers of mixed-ligand assembly have become a very attractive research subject.[1–4] This is not only due to their intriguing structural diversity but also to the intriguing potential applications of functional materials, such as selective molecular recognition and separation, gas storage and separation, absorption, luminescence, molecular magnetism, ion-exchange and heterogeneous catalysis.[5–8] In this context, the predesign and assembly of novel crystalline materials by structure-directing factors, such as central metal ions, organic ligands, the metal–ligand ratio,

Yan'an University Key Laboratory of New Energy & New Functional Materials, Department of Chemistry and Chemical Engineering, Shaanxi Key Laboratory of Chemical Reaction Engineering, Yan'an University, Yan'an, Shaanxi 716000, China. E-mail: ydtangl@126.com; yadxwjj@126.com

† Electronic supplementary information (ESI) available: X-ray crystallographic files in CIF format for **1**–**3**, the details of selected bond lengths/angles (Table S1), and hydrogen bonds for **1** and **3** (Table S2), the 3D supramolecular structure of **1** (Fig. S1), the 1D double-strand chain of **2** view along [010] direction (Fig. S2), the 2D layer structure of **2** (Fig. S3), the 2D layer structure of **3** (Fig. S4), and the TG curves of compounds **1**–**3** (Fig S5–S7). CCDC 1954874–1954876 contains the supplementary crystallographic data for **1**–**3**. For ESI and crystallographic data in CIF or other electronic format see DOI: 10.1039/c9ra07737e

solvents, temperature, pH value, and other factors, have been validated and summarized.[9–12] The mixed-ligand strategy by the judicious choice of various organic linkers has been proven to be highly-efficient for the construction of metal–organic coordination polymers. Among such systems, most outstanding is the incorporation of polycarboxylates and N-donor co-ligands,[13–15] which has successfully been utilized to generate diverse and interesting polymeric networks with potential properties and contributes to refining our knowledge of self-assembly processes. Within polycarboxylate ligands, aromatic polycarboxyl compounds have extensively been documented as multifunctional tectons, owing to their versatile linking capability in virtue of both covalent bonding and supramolecular interactions.[16–18]

In our strategy, multidentate O- or N-donor ligands have also been employed in the construction of coordination polymers. Among the family of organic carboxylate, tripodal carboxylate shows more superiority,[19–21] the ligand 4,4′,4″-s-triazine-2,4,6-tribenzoic acid (H$_3$tatb) as a class example of tripodal ligands has been utilized, and some metal–organic coordination polymers based on H$_3$tatb have also been investigated.[22–28] However, metal–organic coordination polymers based on H$_3$tatb and N-donor ligands have only been investigated scarcely.[29] To explore the influence of N-donor ligands on achieving different dimensional

and topological structures based on tripodal carboxylate ligand, we also employ 1,3-bis(imidazole-1-ylmethyl)benzene(1,3-bimyb), 4,4′-bis(imidazolyl)biphenyl(bimbp), and 1,4-bis(imidazole-1-ylmethyl)benzene(1,4-bimyb) with different conformations as co-ligands. Three cobalt-based coordination polymers [Co(Htatb)(1,3-bimyb)] (**1**), [Co(Htatb)(bimbp)]·DMF (**2**), and [Co(Htatb)(1,4-bimyb)]·H$_2$O (**3**) were synthesized and characterized. In addition, their fluorescent properties and magnetic behavior were also investigated in this paper.

2 Experimental sections

2.1 Materials and chemical analysis

The H$_3$tatb, 1,3-bimyb, bimbp and 1,4-bimyb ligands were purchased in the Jinan Henghua Sci. & Tec. Co., Ltd.; all other reagents and solvents employed were commercially available and used without further purificaion. Elemental analyses were performed with a PerkinElmer 2400 CHN Elemental analyzer. Infrared spectra on KBr pellets were recorded on a Nicolet 170SX FT-IR spectrophotometer in the range 400–4000 cm^{-1}. UV-vis spectra were recorded on a Shimadzu UV-3600 spectrophotometer in the region 200–700 nm. TG analyses were conducted with a Nietzsch STA 449C micro analyzer under atmosphere at a heating rate of 5 °C min^{-1}. X-ray powder diffraction (PXRD) patterns were recorded on a Shimadzu XRD-7000 diffractometer analyzer. The magnetic susceptibilities were obtained on crystalline samples using a Quantum Design MPMS SQUID magnetometer. The fluorescence spectra were studied using a Hitachi F-7100 fluorescence spectrophotometer at room temperature.

2.2 Computational details

All calculations have been processed in Gaussian 03 package.[30] The magnetic isotropic shielding tensors were carried out with the hybrid DFT method on the basis of B3LYP functional.[31] The experimentally determined geometries for the complete structures of compounds **1**–**3** were used for the calculation of the magnetic exchange coupling constants.[32] Neither variation of the geometrical parameters nor the geometry optimization was attempted in this calculation because a small variation in the geometry can have a big effect on the calculated magnetic interaction parameters.

2.3 Synthesis of [Co(Htatb)(1,3-bimyb)] (1)

A mixture of CoCl$_2$·6H$_2$O (0.1 mmol, 0.024 g), H$_3$tatb (0.1 mmol, 0.026 g), 1,3-bimyb (0.1 mmol, 0.024 g) and 8 mL DMF-H$_2$O (V : V = 1 : 1) was stirred for 30 min in air. The mixture was then transferred to a 20 ml airtight glass reactor and kept at 100 °C for 5 days under autogenous pressure, and then cooled to room temperature at a rate of 5 °C h^{-1}. Red crystals of **1** were obtained and washed with DMF and dried in the air (yield: 53% based on Co). Elemental analysis (%). Calcd for C$_{38}$H$_{27}$N$_7$O$_6$Co: C, 61.96; H, 3.69; N, 13.31%. Found: C, 61.64; H, 3.78; N, 13.56%. IR data (KBr cm^{-1}): 3412 (s), 2358 (w), 1711 (s), 1652 (s), 1547 (m), 1502 (m), 1406 (m), 1134 (w), 1072 (w), 837 (m), 765 (m), 672 (w), 585 (w).

2.4 Synthesis of [Co(Htatb)(bimbp)]·DMF (2)

Complex **2** was prepared as for **1** by using bimbp ligand (0.1 mmol, 0.029 g) instead of 1,3-bimyb. Red crystals of **2** were obtained and washed with DMF and dried in the air (yield: 56% based on Co). Elemental analysis. Calcd for C$_{45}$H$_{34}$N$_8$O$_7$Co: C, 63.01; H, 3.99; N, 13.06%. Found: C, 63.17; H, 3.87; N, 13.27%. IR data (KBr cm^{-1}): 3429 (s), 2107 (m), 1714 (s), 1648 (s), 1521 (m), 1454 (s), 1402 (s), 1154 (m), 1018 (w), 872 (m), 765 (m), 669 (m).

2.5 Synthesis of [Co(Htatb)(1,4-bimyb)]·H$_2$O (3)

The procedure is similar to that of **1**, except that the 1,3-bimyb ligand was replaced by 1,3-bimyb ligand (0.1 mmol, 0.024 g), and the mixture was heated at 100 °C for 5 days, and then it was cooled to room temperature at 5 °C h^{-1}. Purple crystals of **3** were obtained and washed with DMF and dried in the air (yield: 54% based on Co). Elemental analysis (%). Calcd for C$_{38}$H$_{29}$N$_7$O$_7$Co: C 60.48, H 3.87, N 12.99; found: C 60.75; H 3.64; N 12.76; IR data (KBr cm^{-1}): 3421 (s), 2374 (w), 1718 (s), 1654 (s), 1560 (m), 1508 (m), 1396 (m), 1234 (w), 1083 (w), 825 (m), 771 (m), 653 (w), 572 (w).

2.6 X-ray crystallographic studies

Diffraction intensities for the three complexes were collected at 293 K on a Bruker SMART 1000 CCD diffractometer employing graphite-monochromated Mo-Kα radiation ($\lambda = 0.71073$ Å). A semi-empirical absorption correction was applied using the SADABS program.[33] The structures were solved by direct methods and refined by full-matrix least-squares on F^2 using the SHELXS 2014 and SHELXL 2014 programs, respectively.[34,35] Non-hydrogen atoms were refined anisotropically and hydrogen atoms were placed in geometrically calculated positions. The crystallographic data for compounds **1**–**3** are listed in Table 1, and selected bond lengths and angles are listed in Table S1.†

3 Results and discussion

3.1 Crystal structures of [Co(Htatb)(1,3-bimyb)] (1)

Single-crystal X-ray analysis reveals that complex **1** shows a double-strand 1D chain structure. The asymmetric unit of **1** consists of one independent Co^{II} ion, one Htatb ligand, one 1,3-bimyb ligand. Each Co^{II} ion coordinates to two nitrogen atoms from two 1,3-bimyb ligand, four carboxylate oxygen atoms from three Htatb ligands, forming a CoN$_2$O$_4$ distorted octahedral geometry (see Fig. 1a). The bond lengths of Co–O/N are in the range of 2.0104(18) Å to 2.0045(17) Å, the O/N–Co–O/N bond angles cover the range of 59.41(6)–177.70(8)°. In compound **1**, the tripodal carboxylate ligands are partly deprotonated and one carboxylate group adopts μ_2–η^1–η^1 bridging mode to link two Co^{II} ions, and another one adopts μ_1–η^1–η^1 chelating mode to link one Co^{II} ion, resulting in a double-strand chain structure (Fig. 1b). The flexible 1,3-bimyb ligand joins the adjoining two Co^{II} ions to form a ring on both sides of a 1D chain, with the Co···Co separation is 4.176 Å. The adjacent chains are joined to generate a 2D layer

Table 1 Crystal data and structural refinement summary of compounds **1–3**

Identification code	**1**	**2**	**3**
Empirical formula	$C_{38}H_{27}N_7O_6Co$	$C_{45}H_{34}N_8O_7Co$	$C_{38}H_{29}N_7O_7Co$
Formula weight	736.59	857.73	754.61
Crystal system	Triclinic	Triclinic	Triclinic
Space group	$P\bar{1}$	$P\bar{1}$	$P\bar{1}$
a (Å)	9.0115(15)	10.004(2)	8.571(2)
b (Å)	10.9375(17)	14.689(4)	11.968(3)
c (Å)	17.301(3)	15.139(4)	16.874(4)
α (°)	94.820(3)	71.253(4)	91.273(3)
β (°)	100.924(3)	87.999(4)	103.657(3)
γ (°)	92.663(3)	89.725(4)	95.169(3)
V (Å^3)	1665.0(5)	2105.2(9)	1673.4(7)
D_c (mg m^{-3})	1.469	1.353	1.498
Z	2	2	2
μ (mm^{-1})	0.576	0.469	0.577
Reflections collected/unique	8424/5817 [$R_{(int)}$ = 0.0139]	10 365/7331 [$R_{(int)}$ = 0.0129]	11 540/6022 [$R_{(int)}$ = 0.0268]
Goodness-of-fit (GOF) on F^2	1.062	1.036	1.033
Final R indices [$I > 2\sigma(I)$]	R_1 = 0.0397 wR_2 = 0.1113	R_1 = 0.0438 wR_2 = 0.1098	R_1 = 0.0498 wR_2 = 0.1302
Largest difference in peak and hole (e Å^{-3})	0.372 and −0.373	0.797 and −0.445	0.714 and −0.567

structure through intermolecular O–H⋯O hydrogen bonds [O3–H3A⋯O4 distance: 2.6478(18) Å, angle: 176.95(4)] (Fig. 1c). Further, through aromatic π–π stacking interactions between phenyl rings of two Htatb ligands (centroid-to-centroid distance: 3.681(3) Å), the adjacent layers generate a 3D supramolecular structure (Fig. S1 in the ESI†).

3.2 Crystal structures of [Co(Htatb)(bimbp)]·DMF (2)

Compound **2** shows a 2D structure with 1D channel, and compound **2** is made up of the Co^{II} ion, Htatb ligand, bimbp ligand and free DMF molecule. Each Co^{II} ion is located in a distorted octahedral geometry and is coordinated to four oxygen atoms of two Htatb ligand and two nitrogen atoms of two bimbp ligands, as shown in Fig. 2a. The bond lengths of Co–O/N are in the range of 2.0394(19)–2.2578(19) Å, the O/N–Co–O/N bond angles cover the range of 59.20(7)–178.24(8)°. As compound **1** is same, the carboxylic groups of Htatb ligand have two coordination modes: one carboxylate group adopts $\mu_2-\eta^1-\eta^1$ bridging mode to link two Co^{II} ions, and another one adopts $\mu_1-\eta^1-\eta^1$ chelating mode to link one Co^{II} ion, resulting in a double-strand chain structure (Fig. S2 in the ESI†). Through bimbp ligands bridging, the adjacent chains are connected to generate a 2D structure with 1D channel (See Fig. 2b and S3†). The potential volume accessible for DMF, determined by PLATON calculation, is 410.3 Å^3 per unit cell volume (2105.2 Å^3), which represents 19.5% void per unit volume for **2**.

3.3 Crystal structures of [Co(Htatb)(1,4-bimyb)]·H$_2$O (3)

Complex **3** exhibits a 4-fold interpenetrating 3D structure. The asymmetric unit of **3** comprises one Co^{II} ion, one Htatb ligand, one 1,4-bimyb ligand and one free water molecule, which is disposed about a centre of inversion. Each four-coordinated Co^{II} center is surrounded by two nitrogen atoms coming from two 1,4-bimyb ligands, and two oxygen

atoms from two Htatb ligands, taking a distorted tetrahedral geometry (Fig. 3a). The bond lengths of Co–O and Co–N are in the range of 1.973(2)–2.040(3) Å. Compared with complexes **1** and **2**, the carboxylic groups of **3** adopts $\mu_1-\eta^1-\eta^0$ and $\mu_1-\eta^1-\eta^0$ bridging mode to link two Co^{II} ions, resulting in a 1D chain structure, through 1,4-bimyb ligand bridging, the adjacent chains are connected to generate a 2D layer structure (Fig. S4†). These 2D layers are further joined by O–H⋯O hydrogen bonding [O5–H5⋯O2 distance: 2.592(3) Å, angle: 176.95(4)] to produce a 3D architecture (Fig. 3b). In order to simplify the 3D framework, we considered the Htatb anion as a 3-connected node and Co^{II} ion as a 5-connected node, 1,4-bimyb ligand as linkers, the whole framework can be simplified as a 3,5-connected 2-nodal net topology with a point symbol of $(3\cdot7^2)(3^2\cdot7^5\cdot8^3)$(Fig. 3c). However, due to the absence of large guest molecules to fill the void space, the potential voids are filled *via* mutual interpenetration of three independent equivalent frameworks, generating a four-fold interpenetrating 3D architecture (Fig. 3d).

3.4 Structural diversity of 1–3

It is noteworthy that a variety of framework structures can be achieved on the basis of the choice of H$_3$tatb and imidazole-containing ligands. From Htatb containing compounds **1–3**, Htatb ligand shows two types of coordination modes: one adopts $\mu_2-\eta^1-\eta^1$ and $\mu_1-\eta^1-\eta^1$ bridging mode for **1** and **2**, another adopts $\mu_1-\eta^1-\eta^0$ and $\mu_1-\eta^1-\eta^0$ bridging mode for **3**, and then the different N-containing co-ligands were employed, resulting in three different dimensional frameworks (compound **1** for 1D, compound **2** for 2D, compound **3** from 2D to 3D). The different imidazole-containing ligands may affect the structure of compounds, when a flexible ligand (1,3-bimyb) is employed to generate 1D structure for **1**, when a rigid ligand (bimbp) is attended, the 2D structure of **2** are obtained, when a semi-rigid ligand is used, a 4-fold interpenetrating 3D architecture for **3** is obtained. By
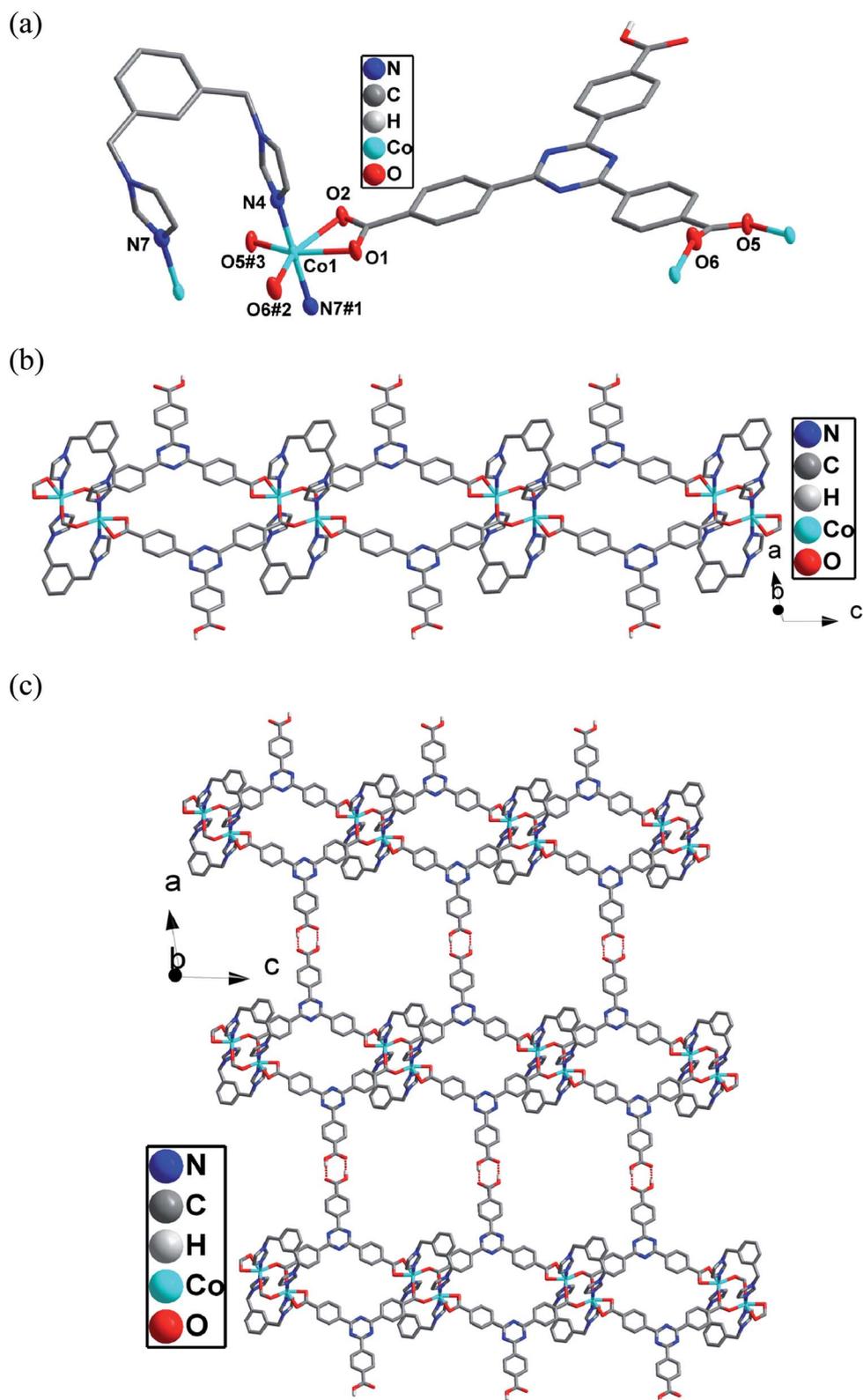
Fig. 1 (a) The coordination environments of Co(ɪɪ) ion in compound **1**. Hydrogen atoms are omitted for clarity except the Htatb ligand. Displacement ellipsoids are drawn at the 50% probability level (symmetry code: #1 −x + 1, −y + 1, −z + 1, #2 x, y, z − 1, #3 −x + 1, −y + 1, −z) (b) The double-strand chain structure of **1**. (c) The 2D layer structure of **1**.
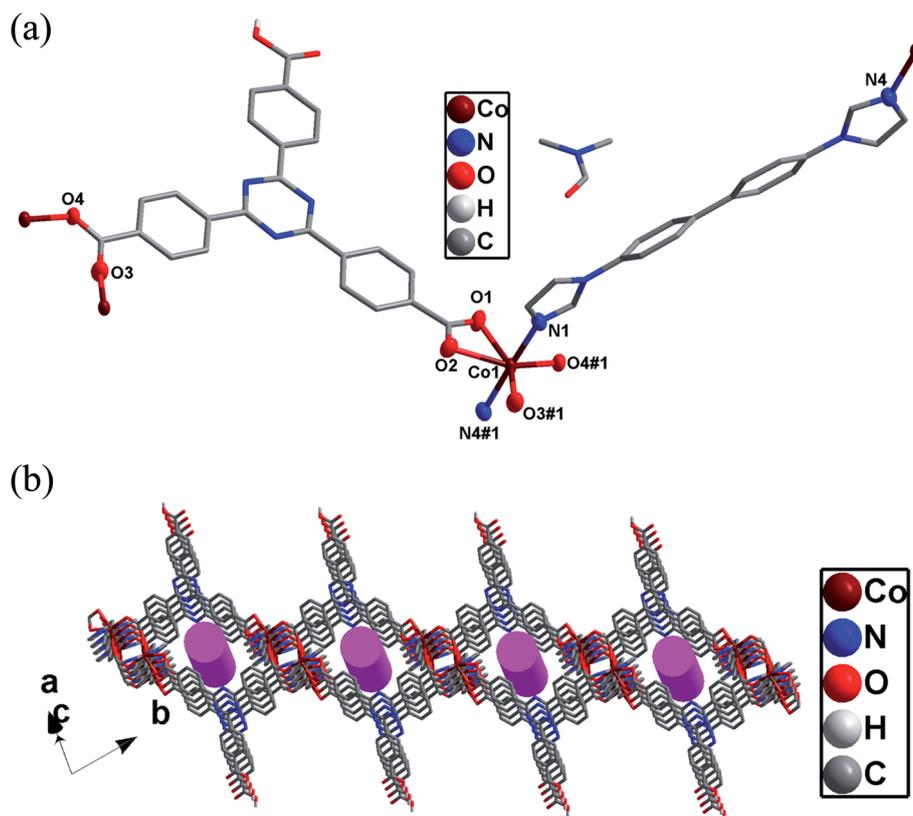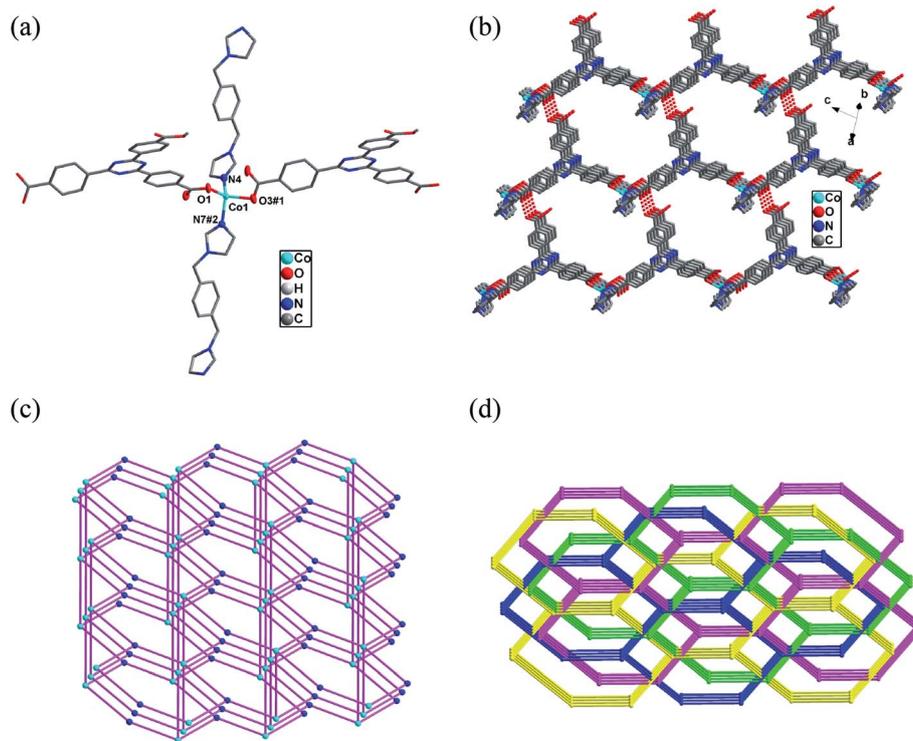
Fig. 2 (a) The coordination environments of Co(II) ion in **2**. Hydrogen atoms are omitted for clarity except the Htatb ligand. (symmetry code: #1 $-x - 1, -y + 1, -z + 2$, #2 $x, y + 1, z - 1$, #3 $x - 1, y, z + 1$). (b) The 2D structure with 1D channel of **2**.

Fig. 3 (a) The coordination environments of Co(II) ion in **3**. Hydrogen atoms are omitted for clarity except the Htatb ligand. (symmetry code: #1 $x + 1, y, z + 1$, #2 $x - 1, y - 1, z$). (b) The 3D architecture of **3**. (c) The 3,5-connected net topology of **3**. (d) The four-fold interpenetrating 3D architecture of **3**.

comparing of the structures of compounds **1–3**, the H_3tatb and imidazole-containing ligands may tune the final structural features.

3.5 Thermogravimetric analysis

To study the thermal stability of **1–3**, thermogravimetric (TG) analyses were performed on polycrystalline samples under a nitrogen atmosphere with a heating rate of 10 °C min^{-1} (see Fig. S5–S7†). The TG curve of **1** reveals that no weight loss occurs from 20 °C until about 220 °C, above which, a significant weight loss of 92.4% is observed and ended at about 460 °C indicating the release the organic ligands (calcd. 92.0%). The TG curve of **2** shows two step weight losses, the first weight loss in the range 50–140 °C (obsd 8.7%, calcd. 8.5%) was assignable to the loss of DMF molecules. The second weight loss of 85.3% in the temperature range 210 to 470 °C corresponds to the release of the Htatb and bimbp ligands (calcd. 84.6%). TG curve of **3** reveals that the first weight loss of 2.6% from 40 °C to 120 °C corresponds to the loss of the lattice water molecules (calcd. 2.4%), and then the larger weight loss(obsd 90.4%) occurred in the range of 230–500 °C, corresponding to the decomposition of the Htatb and 1,4-bimyb ligands (calcd. 89.8%). The final decomposition products of **1–3** were confirmed to be CoO, which have also been further confirmed by PXRD patterns of compounds.

3.6 Infrared spectra of complexes 1–3

IR spectra of complexes **1–3** show features attributable to compositions of the coordination polymers. The observed strong characteristic peaks appearing around 3412, 3429 and 3421 cm^{-1} in spectra are attributed to the O–H stretching vibrations, respectively.[36] Due to partial deprotonation of carboxylate in complexes **1–3**, the absorptions about 1711, 1714 and 1718 cm^{-1} can be attributed to the stretching vibrations of the ν_{COOH} in the carboxylate.[37,38] The presence of the characteristic bands at 1652, 1648 and 1654 cm^{-1} for **1–3** suggest the $\nu_{-C=N-}$ stretching vibrations of Htatb ligand. The intense characteristic peaks appearing around 1547 and 1502, 1406 cm^{-1} for **1**, 1521 and 1454, 1348 cm^{-1} for **2**, 1560 and 1508, 1396 cm^{-1} for **3** in the IR spectra correspond to asymmetric and symmetric stretching vibrations of carboxylic groups, respectively.[39,40] The presence of the characteristic bands at 1134, 1154 and 1234 cm^{-1} for **1–3** suggest the ν_{C-O} stretching vibrations. The presence of the characteristic bands at 1072 cm^{-1} for **1**, 1018 cm^{-1} for **2**, 1083 cm^{-1} for **3** suggest the ν_{C-N} stretching vibrations of the imidazole ring.[41] The presence of the characteristic bands at 1072 cm^{-1} for **1**, 1018 cm^{-1} for **2**, 1083 cm^{-1} for **3** suggest the ν_{C-N} stretching vibrations of the imidazole ring.[42] The absorptions about 650–880 cm^{-1} of **1–3** can be attributed to the ν_{C-H} bending vibrations of phenyl ring.

3.7 UV-vis spectroscopy

The UV-vis spectrum of the free ligands and complexes **1–3** in DMF-H_2O (V : V = 1 : 1) is described in Fig. 4. In the spectra of the H_3tatb ligand, one broad and strong absorption band at 354 nm occurred in the range of 300–400 nm, and the absorption bands of the bimbp, 1,3-bimyb and 1,4-bimyb ligands, found at 335 nm, 391 nm and 386 nm, can be assigned to the $\pi \rightarrow \pi^*$ and n $\rightarrow \pi^*$ transitions of the these ligands. In the spectra of complexes **1** and **3**, the maximum of absorbance are observed at 348 nm (**1**) and 351 nm (**3**), can be assigned to the n $\rightarrow \pi^*$ transitions of the ligands and exhibit slight blue shifted compared to the H_3tatb ligand (354 nm), these shifts reflect coordination of the ligands to the Co(II) atom. The absorption bands of complex **2** was observed at 336 nm (**2**), which can be attributed to the intraligand $\pi \rightarrow \pi^*$ and n $\rightarrow \pi^*$ transitions of the coordinated ligands.

3.8 Photoluminescence properties

The luminescent emission spectra of **1–3** were examined in the solid state at room temperature as is shown in Fig. 5. The main
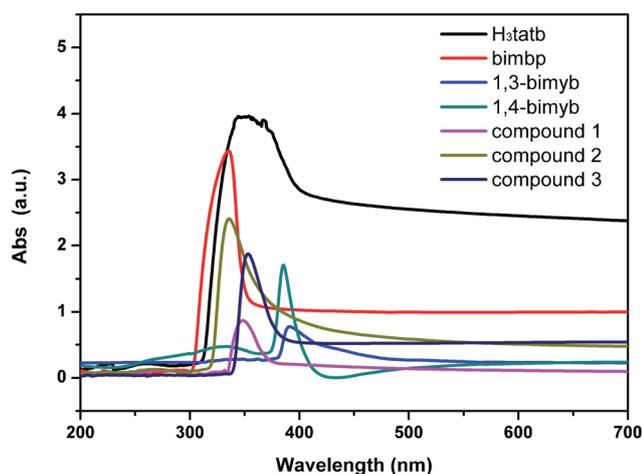

Fig. 4 The UV–vis spectrum of the free ligands and complexes **1–3** in DMF-H_2O (V : V = 1 : 1).
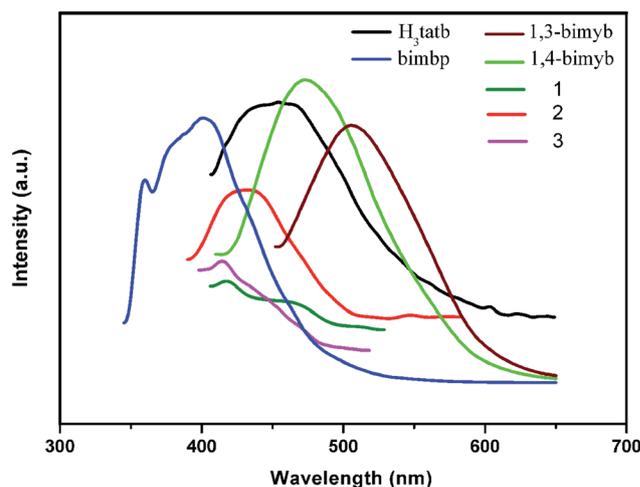

Fig. 5 The solid state luminescent emissions of complexes **1–3** and ligands.

emission peak of the free ligand H$_3$tatb appears at 454 nm (λ_{ex} = 364 nm) and can be assigned to the intra-ligand π^*–π transitions.[43] Complexes **1** and **3** show similar weaker emission peaks at 414 nm and 417 nm (λ_{ex} = 366 nm), however, the intense emission of 1,3-bimyb and 1,4-bimyb ligand were observed at 506 nm (λ_{ex} = 433 nm) and 473 nm (λ_{ex} = 400 nm), respectively. Relative to their ligands, complexes **1** and **3** show a blue shift, probably owing to ligand to metal charge transfer (LMCT).[44,45] Complex 2 show an emission peaks at 432 nm (λ_{ex} = 345 nm), in comparison with that of free H$_3$tatb and bimbp ligand (an intense emission at 401 nm (λ_{ex} = 340 nm)), which are attributed to H$_3$tatb or bimbp ligand-based charge transfer.[46,47]

3.9 Magnetic property

The magnetic susceptibilities (χ_M) of **1** and **2** were measured in the temperature range of 2–300 K with a field of 1000 Oe. To simulate the experimental magnetic behavior, we analyzed the experimental $\chi_M T$ data of **1** and **2** by the dinuclear models as expressed by eqn (1).[48]

$$\chi_M = \frac{2Ng^2\beta^2}{kT}$$

$$\times \frac{\exp(-2J/kT) + 5\exp(-6J/kT) + 14\exp(-12J/kT)}{1 + 3\exp(-2J/kT) + 5\exp(-6J/kT) + 7\exp(-12J/kT)} \quad (1)$$

N, g, β, k and T are the Avogadro number, Zeeman factor, Bohr magneton, Boltzmann constant and temperature in kelvin, respectively. J is the exchange coupling constant between adjacent Co(II) ions.

The magnetic results of complex **1** are illustrated in Fig. 6a. As observed, the experimental $\chi_M T$ value at 300 K is 3.796 cm^3 ·K mol^{-1}, which is somewhat larger than the expected value (3.75 cm^3 ·K mol^{-1}) of the two isolated spin-only Co(II) ions ($S = 3/2$). The distance between two closest Co(II) centers aligned in the 1D chain is 4.176 Å. When the temperature decreases, the $\chi_M T$ descends gradually until 75 K and then rapidly drops to 2 K. The temperature dependence of the reciprocal susceptibility (1/χ_M) obeys the Curie–Weiss law above 30 K with $\theta = -8.44$ K, $C = 3.69$ cm^3 K mol^{-1} and $R = 6.24 \times 10^{-4}$ ($R = \sum[(\chi_M)_{obs} - (\chi_M)_{calc}]^2 / \sum[(\chi_M)_{obs}]^2$). The best fitting for the experimental data was found with $J = -7.27$ cm^{-1}, $g = 2.24$ and $R = 4.13 \times 10^{-4}$. The values of J and θ indicate the antiferromagnetic interactions between adjacent Co(II) ($S = 3/2$) ions.

The experimental $\chi_M T$ values of **2** is 3.713 cm^3 K mol^{-1} at room temperature (Fig. 6b), which are very close to the expected value of 3.75 cm^3 K mol^{-1} for two isolated spin-only Co(II) ions with $S = 3/2$. As the temperature decreases, the $\chi_M T$ value gradually decreases till 50 K to reach a value of 2.73 cm^3 K mol^{-1} after which an obvious fall was appeared to reach a value of 0.03 cm^3 K mol^{-1} at 2 K, manifesting a significant antiferromagnetic exchange between the magnetic centres in Co$_2$ dimer. The temperature dependence of the reciprocal susceptibility (1/χ_M) obeys the Curie–Weiss law above 30 K with $\theta = -7.21$ K, $C = 3.73$ cm^3 K mol^{-1} and $R = 5.17 \times 10^{-4}$. The best-fit parameters for the experimental data gives, $J = -9.42$ cm^{-1}, $g = 2.28$ and $R = 1.14 \times 10^{-4}$. In **2**,

the magnetic coupling between two Co(II) centers is transmitted through two carboxylate bridges, the Co···Co distance of 4.156 Å is responsible for the antiferromagnetic coupling. In these compounds, this behavior indicates a dominant antiferromagnetic interaction between the Co(II) ions for **1** and **2**. However, complex **3** features a 3D supramolecular structure, the Co···Co distances through the Htatb and 1,4-bimyb ligands bridging are 17.026 and 14.079 Å, due to the large distance between adjacent Co(II) ions, we did not discuss the magnetic behavior of **3**.

3.10 Magnetic properties of DFT calculations

The DFT calculations have been widely proved to be one of the most efficient tools to investigate magnetic structure of transition metal complexes.[49–51] We used a phenomenological Heisenberg Hamiltonian $\hat{H} = -J\hat{S}_1\hat{S}_2$ to describe the exchange coupling in a dinuclear compound, the coupling constant J can be related to the energy difference between the lowest and highest spin states. For the case in which $S_1 = S_2$, the coupling constant may be obtained by using the following eqn (3).[52]

$$E_{HS} - E_{LS} = -2JS_i(S_i + 1/2) \quad (2)$$

where E_{HS} is the energy that corresponds to the state with the highest total spin, E_{LS} corresponds to the state with the lowest total spin ($S = 0$), and S_i is the total spin on each metal atom.

When using DFT-based wave functions, a reasonable estimate of the energy corresponding to the low spin state, E_{LS} can be obtained directly from the energy of a broken-symmetry solution E_{BS}. In this case, compounds **1** and **2** are 1D chain and 2D layer, and the theoretical calculations would be a difficult task for such a large periodical system. Here, the monomer [Co$_2$(Htatb)$_2$(1,3-bimyb)$_2$] of **1** [Co$_2$(Htatb)$_2$(bimbp)$_2$] of **2** were intercepted, we arrive to the following expressions for J:

$$E_{HS} - E_{BS} = -6J_{Co–Co} \quad (3)$$

The calculated coupling constant J and related quantities are listed in Table 2. We have used via eqn (3) to estimate the magnetic coupling constants (J) of compounds **1** and **2**. The computed J values ($J = -9.04$ cm^{-1} for **1** and $J = -11.63$ cm^{-1} for **2**) predict antiferromagnetic, the results were agreed with the experimental data. We have used the non-spin projected, giving a better agreement for compounds **1** and **2**. This is due to the strong localization of the wavefunction at the metal centers both computational techniques produce results that are in remarkable agreement with the experimental value. Full molecule calculation using hybrid B3LYP functional to reproduce BS–HS energy gap of compounds is not only found to be successful in describing the magnetic behavior of the compounds correctly in this study but also yielded J that are in excellent agreement with the experimental value. So the full molecule DFT based calculation based on X-ray structural data could be successfully used to rationalize the magnetic behavior of this class of compounds.
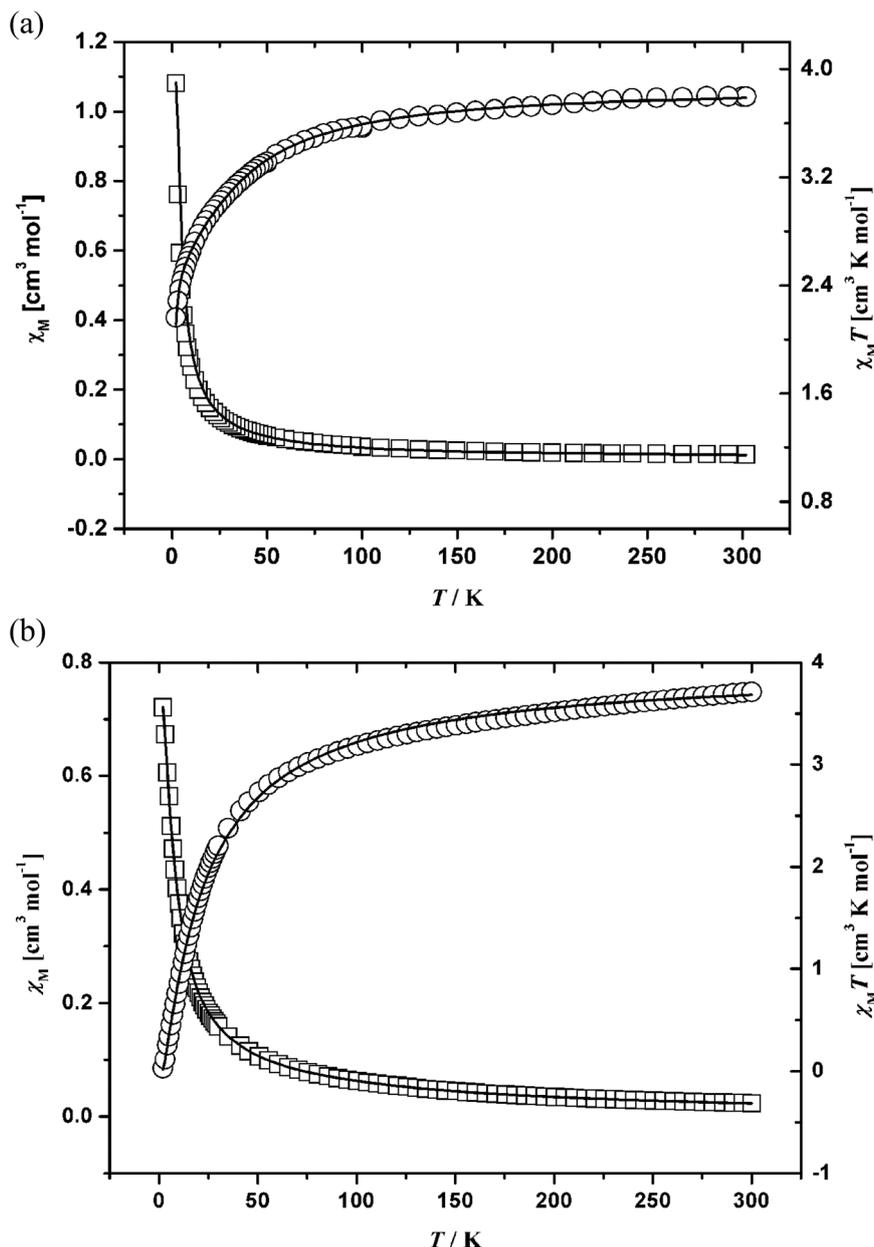
Fig. 6 Thermal variation of χ_M and $\chi_M T$ for **1** (a) and **2** (b) ($\bigcirc$, χ_M experimental values, $\square$, $\chi_M T$ experimental values and the solid line represents the best fit obtained from the Hamiltonian given in the text.).

Table 2 Calculated energy (au.) and magnetic exchange constant J (cm^{-1}) for **1** and **2**

Compound	E_{BS}/(au.)	E_{HS}/(au.)	Calculation, J/(cm^{-1})	Experiment, J/(cm^{-1})
1	−9684.132164	−9684.131917	−9.04	−7.27
2	−10160.989084	−10160.988766	−11.63	−9.42

4 Conclusions

In summary, three cobalt-based coordination polymers have been synthesized by the self-assembly of Co(II) salts with H_3tatb and imidazole-containing Ligands. Assemblies of these compounds generate three types of diverse frameworks: one 1D chain, one 2D layer and 2D to 3D structure. By comparing of the structures of **1–3**, the N-donor ligand can also slightly tune the final structural features. Moreover, the fluorescent properties of **1–3** and magnetic behavior of **1** and **2** have also been investigated. According to the crystal structures, the DFT-BS approach was applied to study the magnetic coupling behavior for **1** and **2**, the result reveals that the calculated exchange coupling constants J were in good agreement with the experimental data.

Conflicts of interest

There are no conflicts to declare.

Acknowledgements

References

1 Y. P. Wu, W. Zhou, J. Zhao, W. W. Dong, Y. Q. Lan, D. S. Li, C. H. Sun and X. H. Bu, *Angew. Chem., Int. Ed.*, 2017, **56**, 13001–13005.

2 Q. G. Zhai, X. H. Bu, X. Zhao, D. S. Li and P. Y. Feng, *Acc. Chem. Res.*, 2017, **50**, 407–417.

3 Y. Zhao, X. G. Yang, X. M. Lu, C. D. Yang, N. N. Fan, Z. T. Yang, L. Y. Wang and L. F. Ma, *Inorg. Chem.*, 2019, **58**, 6215–6221.

4 G. Wang, Q. Sun, Y. Liu, B. Huang, Y. Dai, X. Zhang and X. Qin, *Chem.–Eur. J.*, 2015, **21**, 2364–2367.

5 Y. L. Wang, J. H. Fu, J. J. Wei, X. Xu, X. F. Li and Q. Y. Liu, *Cryst. Growth Des.*, 2012, **12**, 4663–4668.

6 D. S. Li, J. Zhao, Y. P. Wu, B. Liu, L. Bai, K. Zou and M. Du, *Inorg. Chem.*, 2013, **52**, 8091–8098.

7 Y. Zhao, L. Wang, N. N. Fan, M. L. Han, G. P. Yang and L. F. Ma, *Cryst. Growth Des.*, 2018, **18**, 7114–7121.

8 H. R. Fu, N. Wang, J. H. Qin, M. L. Han, L. F. Ma and F. Wang, *Chem. Commun.*, 2018, **54**, 11645–11648.

9 X. Y. Zhang, B. Li and J. P. Zhang, *Inorg. Chem.*, 2016, **55**, 3378–3383.

10 I. H. Park, R. Medishetty, J. Y. Kim, S. S. Lee and J. J. Vittal, *Angew. Chem., Int. Ed.*, 2014, **53**, 5591–5595.

11 S. Q. Chen, Q. G. Zhai, S. N. Li, Y. C. Jiang and M. C. Hu, *Inorg. Chem.*, 2015, **54**, 10–12.

12 Y. He, W. Zhou, G. Qian and B. Chen, *Chem. Soc. Rev.*, 2014, **43**, 5657–5658.

13 M. G. Campbell, D. Sheberla, S. F. Liu, T. M. Swager and M. Dinca, *Angew. Chem., Int. Ed.*, 2015, **54**, 4349–4352.

14 K. Manna, T. Zhang, F. X. Greene and W. Lin, *J. Am. Chem. Soc.*, 2015, **137**, 2665–2673.

15 L. L. Shen, L. Yang, Y. Fan and L. Wang, *CrystEngComm*, 2015, **17**, 9363–9369.

16 W. Lin, Y. Cui, Y. Yu, Q. Hu and G. Qian, *Dalton Trans.*, 2018, **47**, 15882–15887.

17 Y. J. Cheng, R. Wang, S. Wang, X. J. Xi, L. F. Ma and S. Q. Zang, *Chem. Commun.*, 2018, **54**, 13563–13566.

18 Z. J. Lin, J. Lv, M. C. Hong and R. Cao, *Chem. Soc. Rev.*, 2014, **43**, 5867–5895.

19 Y. W. Li, H. Ma, Y. Q. Chen, K. H. He, Z. X. Li and X. H. Bu, *Cryst. Growth Des.*, 2012, **12**, 189–196.

20 J. P. Zhang, Y. B. Zhang, J. B. Lin and X. M. Chen, *Chem. Rev.*, 2012, **112**, 1001–1033.

21 M. P. Suh, H. J. Park, T. K. Prasad and D. W. Lim, *Chem. Rev.*, 2012, **112**, 782–835.

22 S. Q. Ma, D. F. Sun, M. Ambrogio, J. A. Fillinger, S. Parkin and H. C. Zhou, *J. Am. Chem. Soc.*, 2007, **129**, 1858–1859.

23 S. Q. Ma, X. S. Wang, D. Q. Yuan and H. C. Zhou, *Angew. Chem., Int. Ed.*, 2008, **47**, 4130–4133.

24 W. Gao, F. F. Xing, D. Zhou, M. Shao and S. R. Zhu, *Inorg. Chem. Commun.*, 2011, **14**, 601–605.

25 H. B. Zhang, N. Li, C. B. Tian, T. F. Liu, F. L. Du, P. Lin, Z. H. Li and S. W. Du, *Cryst. Growth Des.*, 2012, **12**, 670–678.

26 J. W. Rong, W. W. Zhang and J. F. Bai, *CrystEngComm*, 2016, **18**, 7728–7736.

27 C. S. Liu, Z. H. Zhang, M. Chen, H. Zhao, F. H. Duan, D. M. Chen, M. H. Wang, S. Zhang and M. Du, *Chem. Commun.*, 2017, **53**, 3941–3944.

28 X. Duan, R. Lv, Z. G. Ji, B. Li, Y. J. Cui, Y. Yang and G. D. Qian, *Inorg. Chem. Front.*, 2018, **5**, 1193–1198.

29 X. B. Liu, Z. Y. Xiao, A. Huang, W. Wang, L. L. Zhang, R. M. Wang and D. F. Sun, *Z. Anorg. Allg. Chem.*, 2016, **642**, 31–35.

30 M. J. Frisch, G. W. Trucks, H. B. Schlegel, G. E. Scuseria, M. A. Robb, J. R. Cheeseman, Jr, J. A. Montgomery, T. Vreven, K. N. Kudin, J. C. Burant, J. M. Millam, S. S. Iyengar, J. Tomasi, V. Barone, B. Mennucci, M. Cossi, G. Scalmani, N. Rega, G. A. Petersson, H. Nakatsuji, M. Hada, M. Ehara, K. Toyota, R. Fukuda, J. Hasegawa, M. Ishida, T. Nakajima, Y. Honda, O. Kitao, H. Nakai, M. Klene, X. Li, J. E. Knox, H. P. Hratchian, J. B. Cross, V. Bakken, C. Adamo, J. Jaramillo, R. Gomperts, R. E. Stratmann, O. Yazyev, A. J. Austin, R. Cammi, C. Pomelli, J. W. Ochterski, P. Y. Ayala, K. Morokuma, G. A. Voth, P. Salvador, J. J. Dannenberg, V. G. Zakrzewski, S. Dapprich, A. D. Daniels, M. C. Strain, O. Farkas, D. K. Malick, A. D. Rabuck, K. Raghavachari, J. B. Foresman, J. V. Ortiz, Q. Cui, A. G. Baboul, S. Clifford, J. Cioslowski, B. B. Stefanov, G. Liu, A. Liashenko, P. Piskorz, I. Komaromi, R. L. Martin, D. J. Fox, T. Keith, M. A. Al-Laham, C. Y. Peng, A. Nanayakkara, M. Challacombe, P. M. W. Gill, B. Johnson, W. Chen, M. W. Wong, C. Gonzalez and J. A. Pople, *Gaussian 03, Gaussian(version 6.1)*, Inc., Wallingford CT, 2004.

31 A. D. Becke, *J. Chem. Phys.*, 1997, **107**, 8554–8560.

32 E. Ruiz, A. Rodríguez-Fortea, J. Tercero, T. Cauchy and C. J. Massobrio, *Chem. Phys.*, 2005, **123**, 074102.

33 G. M. Sheldrick, *SADABS, A Program for Empirical Absorption Correction of Area Detector Data*, University of Göttingen, Germany, 1997.

34 G. M. Sheldrick, *SHELXS-2014/7, Program for Crystal Structure Solution*, University of Göttingen, Germany2014.

35 G. M. Sheldrick, *SHELXL-2014/7, Program for Crystal Structure Refinement*, University of Göttingen, Germany2014.

36 P. S. Kalsi, *Spectroscopy of Organic Compounds*, New Age International, New Delhi, 2008.

37 I. Mohammed-Ziegler and A. Grün, *Spectrochim. Acta, Part A*, 2005, **62**, 506–517.

38 I. Mohammed-Ziegler, A. Hamdi, R. Abidi and J. Vincens, *Supramol. Chem.*, 2006, **18**, 219–234.

39 B. Dolenský, R. Konvalinka, M. Jakubek and V. Král, *J. Mol. Struct.*, 2013, **1035**, 124–128.

40 S. Mandal, G. Das and H. Askari, *Struct. Chem.*, 2014, **25**, 43–51.

41 L. J. Bellamy, *The Infrared Spectra of Complex Molecules*, Wiley, New York, 1958.

42 G. Świderski, A. Z. Wilczewska, R. Świsłocka, M. Kalinowska and W. Lewandowski, *J. Therm. Anal. Calorim.*, 2018, **134**, 513–525.

43 Y. Gong, Z. Hao, J. L. Sun, H. F. Shi, P. G. Jiang and J. H. Lin, *Dalton Trans.*, 2013, **42**, 13241–13250.

44 Y. Q. Xu, D. Q. Yuan, B. L. Wu, L. Han, M. Y. Wu, F. L. Jiang and M. C. Hong, *Cryst. Growth Des.*, 2006, **6**, 1168–1174.

45 Y. J. Cui, Y. F. Yue, G. D. Qian and B. L. Chen, *Chem. Rev.*, 2012, **112**, 1126–1162.

46 X. P. Yang, S. Q. Wang, L. J. Zhang, S. M. Huang, Z. P. Li, C. R. Wang, T. Zhu and L. Bo, *J. Mater. Chem. C*, 2016, **4**, 1589–1593.

47 B. C. Yuan, F. Wang, J. B. Tao, M. Li and X. P. Yang, *Inorg. Chim. Acta*, 2019, **490**, 24–28.

48 O. Kahn, *Molecular Magnetism*, VCH Publishers Inc, New York, 1993.

49 L. Tang, F. Fu, J. J. Wang, L. J. Gao, D. D. Chao and Z. Wang, *Polyhedron*, 2015, **88**, 116–124.

50 C. Beghidja, G. Rogez, J. Kortus, M. Wesolek and R. Welter, *J. Am. Chem. Soc.*, 2006, **128**, 3140–3141.

51 E. Ruiz, P. Alemany, S. Alvarez and J. Cano, *Inorg. Chem.*, 1997, **36**, 3683–3688.

52 A. Rodríguez-Fortea, P. Alemany, S. Alvarez and E. Ruiz, *Inorg. Chem.*, 2001, **40**, 5868–5877.